PRESIDENTIAL ADDRESS

Lithologic partitioning of fluids and melts

E. BRUCE WATSON*

Department of Earth and Environmental Sciences, Rensselaer Polytechnic Institute, Troy, New York 12180, U.S.A.

ABSTRACT

Under conditions of mechanical equilibrium, the grain-scale distribution of fluid or melt in a lithologically complex system is governed by the relative energies of the mineral-fluid interfaces and the grain boundaries. Accordingly, spatial changes in mineralogy imply accompanying changes in the connectivity and even the amount of fluid (or melt) present at equilibrium. The hypothesized phenomenon of local variation in fluid or melt abundance with spatial changes in mineralogy is referred to here as *lithologic partitioning* of fluid or melt. The phenomenon is potentially important because it could lead to the existence of highly permeable (or impermeable) zones in lithologically complex regions of the crust and upper mantle.

To verify and evaluate the concept of lithologic partitioning of aqueous fluid, experiments were conducted in simple analog systems by annealing juxtaposed cylinders of two different rock types at 700–925 °C and 1.0–1.5 GPa. These polycrystalline fluid partition couples included the following rock pairs: calcite-fluorite, quartz-fluorite, and quartz-clinopyroxene, with overall aqueous fluid volume fractions (ϕ) ranging from ~0.015 to 0.10. In calcite-fluorite couples, fluid is partitioned by a factor of ~1.5–5 into the fluorite (the actual value depends upon the chemical purity of the fluorite). In fluorite-quartz couples, the fluid is partitioned into the quartz by a factor of 2–5, and in quartz-clinopyroxene couples it is enriched in the clinopyroxene by a factor of ~3. Similar experiments were done in a partially molten mantle system by juxtaposing peridotite and orthopyroxenite cylinders in the presence of ~6% basaltic melt. In this case, however, no preference of the melt for one host rock relative to the other could be verified. In general, lithologic partitioning is a factor to be reckoned with as we seek understanding of fluid-related petrologic and geochemical phenomena: the effect is clearly capable of rapid and significant re-distribution and localization of fluids in mineralogically variable systems.

INTRODUCTION

Both the physical and the chemical aspects of fluid (or melt) transport in the crust and upper mantle are strongly determined by the distribution of the fluid phase in the host rock. Uniform dispersal of a small amount of fluid on the scale of mineral grains, for example, may tend to minimize the permeability of the host rock, while at the same time leading to relatively effective chemical equilibration between the fluid and the individual mineral grains. Localization of fluids on a scale significantly larger than the grains may, in contrast, lead to higher permeability but relatively ineffective chemical exchange.

The actual distribution of fluids in localized regions of the deep crust and upper mantle is not directly observable, so our conceptualizations of fluid distribution and behavior are often poorly constrained. In general, our ideas are formed in one of two ways: either they (1) conform to observations made on rocks at the Earth's surface; or (2) constitute manageable starting points for certain types of physical models. Geochemical studies of rocks in the field reveal that in some cases fluid flow can be concentrated within specific units that are appropriately thought of as metamorphic aquifers (e.g., Ferry 1988; see also Kelemen et al. 1995 for a magmatic perspective). In a similar vein, Ague (1995) has documented features indicating segregation of metamorphic fluids at mid-crustal conditions into cavities up to several centimeters in size. Mathematical treatments of melt or fluid flow, in contrast, are commonly predicated on the assumption of uniform, grain-scale dispersal of fluid throughout the region of interest (e.g., Richter and McKenzie 1984; McKenzie 1987). As different as they are, these two images of fluid distribution (non-uniform vs. uniform) are not necessarily in conflict—both may be accurate but applicable to different systems and circumstances. It is even possible that a transition occurs during the evolution of a specific system from one type of fluid distribution to another. Given the range of behavior possible for deep-seated geologic fluids, there is a clear need for constraints on the processes and factors that lead to localization or dispersal of fluids and melts.

Experimental approaches can address some aspects of the

*E-mail: watsoe@rpi.edu

fluid distribution problem. Direct characterization of actual production and flow of fluids has been elusive (due mainly to difficulties in simulating the processes of interest in a geologically plausible manner), but indirect laboratory constraints on fluid behavior do exist. For example, the principles of polycrystalline microstructure (e.g., Smith 1964) prompted experimentalists working on Earth materials to measure fluid-crystal dihedral angles (see theory section below) in simple rock analogs quenched from geologic *P-T* conditions (e.g., Waff and Bulau 1979; Watson and Brenan 1987; Lee et al. 1991; Holness and Graham 1991; Faul et al. 1994; Mibe et al. 1998). These data have shed light on fluid-phase distribution and connectivity in monomineralic aggregates, even though application to realistic, polymineralic rocks (apart from the olivine-dominated mantle) is not straightforward. Dihedral-angle and connectivity information has recently been supplemented by direct measurements of permeability of microstructurally equilibrated, monomineralic rock analogs having fluid fractions in the ~0.01–0.2 range (Wark and Watson 1998); again, however, the usefulness of these data in modeling complex lithologies is not yet clear due to the textural complexities of polymineralic aggregates.

A potentially important piece of the fluid distribution puzzle concerns the inherent tendency of fluids to become concentrated or localized in contact with some minerals relative to others in systems of variable mineralogy—a tendency referred to here as fluid partitioning. The purpose of this paper is to present the results of an experimental study of this phenomenon, which was conducted with two specific objectives in mind: (1) to confirm the principle of fluid partitioning using simple, well-behaved materials (that is, materials known from previous experience to reach a state of microstructural equilibrium within a realistic laboratory time frame); and (2) to explore fluid partitioning in simple rock analogs that are less easily equilibrated but more directly relevant to the Earth. Throughout the paper, the term fluid is used in its broadest sense, referring to any low-viscosity, interactive phase in which components of the polycrystalline host are soluble. The term fluid thus includes melts as well as C-O-H fluids. The principles discussed are equally applicable to both, even though most of the experiments focus on aqueous fluids specifically. Deformation of the solid phase is not a factor in this study: the mineral-fluid microstructures are determined solely by minimization of interfacial energy in the system.

THEORY

Minimum-energy fluid fraction

Before discussing the principles involved in fluid partitioning, it is instructive to consider the interfacial energetics of a system consisting of a single crystalline phase plus fluid in varying proportions. Jurewicz and Watson (1985) and, independently, Park and Yoon (1985) introduced the concept of a *minimum-energy melt fraction* (MEMF) in a system consisting of crystals and melt (the term used by Jurewicz and Watson was actually *equilibrium* melt fraction, but this was later abandoned in favor of the less ambiguous MEMF; see Lupulescu and Watson 1999). For the purposes of this paper, the term should be broadened to *minimum-energy fluid fraction*, in recognition of the general usage here. This term refers to a spe-

cific fluid fraction or porosity (ϕ_m) that corresponds to a minimum in the total interfacial energy of the system, given by the sum of grain-boundary energy (γ_{gb}) and the crystal/fluid interfacial energy (γ_{cf}). A given fluid-rock system is more stable at ϕ_m than at any other fluid fraction (assuming thermodynamic equilibrium among all phases in terms of the volume free energies). The discussion of Jurewicz and Watson (1985) focused on migmatites, and it was suggested that systems in which the minimum-energy melt fraction is exceeded might exhibit segregation of felsic melt even under conditions of chemical and mechanical equilibrium. The ϕ_m principle is illustrated in Figure 1a, where the quantity γ_T plotted against volumetric fluid fraction (ϕ) is the total interfacial energy in a fluid-bearing (wet) rock normalized to the fluid-absent (dry) case, i.e.:

$$\gamma_T = \frac{\gamma_{gb} \cdot A_{gb} + \gamma_{cf} \cdot A_{cf}}{(\gamma_{gb} \cdot A_{gb})_{dry}} \tag{1}$$

where the subscripted A terms refer to the total area of the two general types of interface present in the system (grain boundary or crystal/fluid interface). Figure 1a, modified from Park and Yoon (1985), represents an idealized material containing one solid phase plus fluid—i.e, a material we can use as a model for a fluid-bearing, monomineralic rock. The curves in the figure were calculated using the well-known relationship among γ_{gb}, γ_{cf}, and the dihedral angle, θ, formed at the junction of two crystal/fluid boundaries with a grain boundary:

$$\frac{\gamma_{gb}}{2\gamma_{cf}} = \cos\left(\frac{\theta}{2}\right) \tag{2}$$

[see Kingery et al. (1976) p. 213–214 and Fig. 1b]. Additional assumptions include constant curvature of the crystal/fluid interface and 12 neighbors for each solid grain (all grains the same size). As shown in Figure 1, the value of ϕ_m depends on the dihedral angle θ, but the minimum itself is a consistent feature of the γ_T vs. ϕ curves for θ ranging from 0° to ~80°. It is important to note that both the location of the minimum and the relative changes in γ_T are sensitive to the specific geometric model chosen for calculation. In contrast to Park and Yoon (1985), for example, Jurewicz and Watson (1985) used a simple, two-dimensional geometric model (essentially a 2-D honeycomb of hexagonal grains) to demonstrate the principle of a minimum-energy fluid fraction. Their calculated ϕ_m values are a factor of two or three lower than those resulting from the 3-D model of Park and Yoon (1985) shown in Figure 1. No matter what model geometry is assumed, however, ϕ_m itself is a robust phenomenon, even if its numerical value is model-dependent. Accordingly, it can be safely assumed that ϕ_m is a real feature of complex geologic systems, although we have no knowledge of its actual value in most cases [see Lupulescu and Watson (1999) for an estimate of ϕ_m in a system consisting of felsic melt and amphibolite].

Fluid partitioning

The concept of a minimum-energy fluid fraction has interesting implications for fluid behavior in the Earth. Unfortunately, however, complexities exist in natural systems that are not taken into account in Figure 1, the most important of which may be that a monomineralic system is not an adequate repre-

sentation of a typical rock at any scale. Grain-boundary and crystal-fluid interfacial energies (and θ) are mineral-specific, so γ_T and ϕ_m vary with the identity of the crystalline phase even when only one is present in the system. This observation implies that, in a system of spatially variable mineralogy, ϕ_m will vary with position in the system. There should, accordingly, be some tendency for fluid in a mineralogically complex system to assume a non-uniform distribution on a scale comparable with the non-uniformity in mineralogy. In simple terms, this could mean localization of fluid around or among mineral grains characterized by low γ_{cf}.

Despite its illustrative value, the concept of a minimum-energy fluid fraction is difficult to apply to a system of spatially variable mineralogy. Consider, for example, the extreme case of a system consisting of two halves, both monomineralic but different from one another. If the system is in chemical equilibrium and closed (i.e., overall ϕ fixed)—and if fluid segregation does not occur—it is impossible for ϕ_m to be achieved in both halves simultaneously, except in the fortuitous case that the amount of fluid in the system is equivalent to that required for ϕ_m to be met exactly in both halves. It seems likely instead that the fluid will become distributed (partitioned) between the two halves to minimize the overall interfacial energy of the system. This hypothetical phenomenon of non-uniform (equilibrium) fluid distribution in a complex system is referred to in this paper as *lithologic partitioning* of fluid. In a system of two juxtaposed rock units of markedly different mineralogy (even ones differing only in relative abundance of the same minerals), a non-uniform distribution of fluid is a logical consequence of interfacial energy minimization.

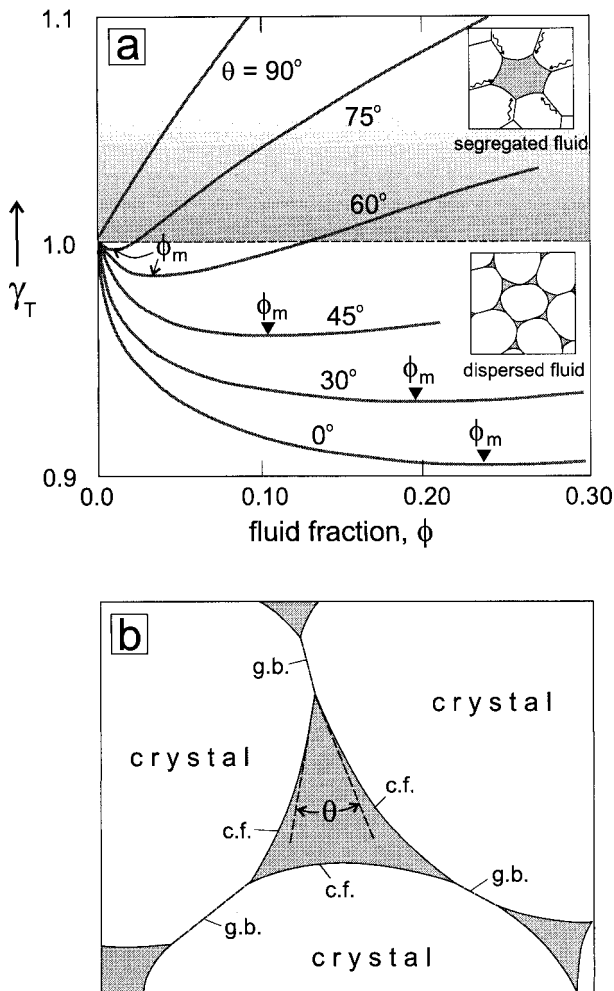Figure 2 shows a hypothetical case of two such rock units (a and b), one characterized by a low average dihedral angle (θ_{avg}),

FIGURE 1. (a) Normalized total interfacial energy, γ_T, of an idealized, monomineralic rock plotted against fluid fraction, ϕ, for various dihedral angles (θ). ϕ_m is the minimum-energy fluid fraction; see text for explanation and Equation 1 for explicit definition of γ_T. [(Figure modified from Park and Yoon 1985). (b) Illustration of crystal-fluid (c.f.) and grain-boundary (g.b.) interfaces and the dihedral angle (θ).
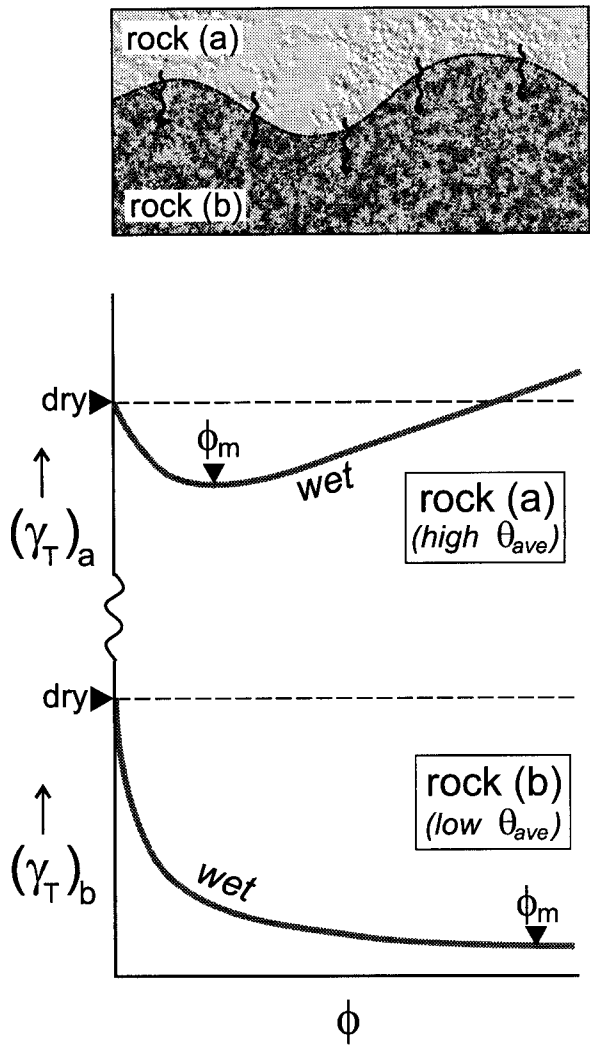

FIGURE 2. Schematic illustration of fluid behavior when two rock units (a and b) having different interfacial energy (γ) characteristics are juxtaposed; see text for explanation.

the other by a relatively high θ_{avg}. It is reasonable to suppose that fluid added to this two-rock system would partition initially into rock b, because a larger apparent reduction in γ_T is achieved as a consequence of the steeper initial (–) slope on the γ_T vs. ϕ curve for this rock (due to the lower θ_{avg}; see Fig. 1). It is reasonable, also, to suppose that any amount of fluid present in the two-rock system will partition in such a way that the sum $(\gamma_T)_a + (\gamma_T)_b$ is minimized. While this is probably true, no attempt is made, even schematically, to illustrate the case on the figure, because even the relative positions of the fluid-absent γ_T values for rocks a and b are unknown. The fact that rock a is assigned a higher θ_{avg} does not necessarily mean that $(\gamma_T)_a$ lies above $(\gamma_T)_b$ in an absolute sense. Recall that, for any given mineral, θ is determined by the relative values of γ_{gb} and γ_{cf} (see Eq. 2). Even if θ is actually measured for a given mineral-fluid system, the absolute values of the interfacial energies remain obscure. Without knowledge of the actual energies involved, it is not possible to determine the relative positions of the "rock a" and "rock b" curves in Figure 2 on a single γ_T scale, or even to know the relative slopes of the curves at any value of ϕ. Figure 2 is thus useful only in an abstract, conceptual sense. While absolute values for the interfacial energies in rocks a and b could be assumed and the arguments developed in greater detail, there would be little gained by such an exercise because knowledge of γ_{gb} and γ_{cf} in real rocks is virtually nonexistent. Suffice it to say that curves such as those shown in Figures 1 and 2, which are a type of free energy vs. composition curve, do not have the same graphical significance as the volume free energy vs. composition curves more familiar to petrologists and geochemists. In fluid partitioning of the type described here, there does not seem to be any requirement of Henry's law behavior, or that the partition coefficient remain constant over changes in bulk fluid fraction in the system. The only firm prediction from the above analysis is that any fluid present in a mineralogically variable system should tend to localize in contact with some minerals in preference to others. This prediction applies not only to the separate rock units shown schematically in Figure 2 but also to individual mineral grains within a given rock.

Besides the considerations noted above, several additional factors will hinder prediction of fluid partitioning behavior in a given petrologic system. These factors include the following.

(1) The effect of grain *faceting* on overall equilibrium microstructure. In at least some systems, θ alone does not determine pore geometry. In some cases pore shape and size are strongly influenced by the tendency of the grains to minimize their interfacial energy (against the fluid) by forming facets (Waff and Faul 1992). In such cases, Figure 1—and the ϕ_m concept in general—are of questionable value. Because a facet is a particularly low-energy crystal/fluid interface, it is possible that fluid will localize around minerals that tend to form facets.

(2) The role of *grain size* in interfacial energy minimization. Jurewicz and Watson (1985) noted that a fluid-bearing rock at ϕ_m is metastable relative to the same rock with a coarser grain size (because the coarser rock has less grain boundary area). Moreover, in a system consisting of two fluid-bearing rocks that are identical in every respect except grain size (and in which faceting does not occur), the fluid should partition into the rock with the smaller grain size. In principle, the equi-

librium requirement of constant curvature of the mineral/fluid interface, in combination with the geometric constraints of the system, will necessitate higher ϕ in finer-grained regions.

(3) The influence of *solutes* and *impurities* upon interface energetics. Watson and Brenan (1987) showed that θ in a system consisting of quartz + aqueous fluid is sensitive to the presence of other solutes in the fluid (see also Lee et al. 1991 and Holness 1995, as well as the discussion below concerning fluorite in quartz-bearing vs. quartz-free systems). It is also generally known that impurities can affect grain-boundary energies (see chapter 5 of Kingery et al. 1976). For these reasons, characterizations of interfacial energies widely relevant to petrologic systems may be slow to develop.

In the face of all these difficulties with theoretical predictions, there is every reason to turn to experiments, at least for validation of the basic idea of lithologic partitioning.

EXPERIMENTAL APPROACH AND TECHNIQUES

General strategy

Most of the experiments performed in this study conform quite closely to the hypothetical case described above in which two fluid-bearing rock units of differing mineralogy are juxta-
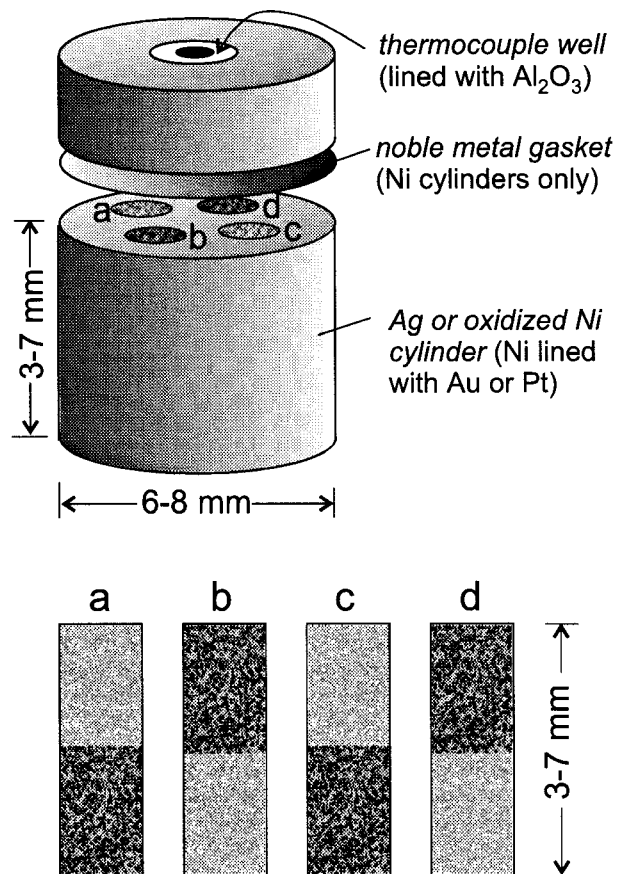

FIGURE 3. Capsule schematic and sample arrangement for partitioning experiments involving aqueous fluids (see text).

posed. The approach was simply to fill the top and bottom halves of a cylindrical container with different minerals, add fluid (usually H_2O) at the level of ~1.5–9 vol% overall, and hold the resulting partition couple at high temperature and pressure to allow the fluid to assume an equilibrium distribution between the two halves. The method is illustrated schematically in Figure 3, which reveals some additional design characteristics of the partition couples. In most cases, two to four individual couples were run simultaneously, contained within individual holes or sleeves inserted or drilled into a larger cylinder (usually metal), which was run vertically in a 19 mm piston-cylinder assembly (NaCl+Pyrex+MgO and/or Al_2O_3). The multiple sleeves enabled several versions of the same couple—in most cases varying only in fluid abundance—to be run at exactly the same conditions. In such an assembly, the "rocks" in the top and bottom positions were alternated in order to ensure that neither gravity nor temperature variation along the cylinder axes (possibly up to 10 °C) played any role in producing the fluid distribution observed at the end of the experiment. Partition experiments involving aqueous fluids were made at 1.0–1.5 GPa and temperatures in the range 700–925 °C for durations ranging from negligible (i.e., zero-time experiments) to about 2 weeks. Experiments involving peridotite and basaltic melt (see below) were run at 1300–1325 °C and 1.5 GPa.

A few experiments of somewhat different design were carried out in addition to the two-lithology, partition-couple type described above. These included couples in which only the starting grain size (not the identity of the minerals) in the two halves of a container was varied. Also included were experiments on uniform "rocks" (as opposed to couples) in which a small amount of a second crystalline phase was introduced into a nearly monomineralic sample to assess the possibility of H_2O localization around the second phase (see below). In all, 30 separate experiments were carried out, incorporating 95 individual couples or samples. The experimental details are summarized in Table 1, which includes all experiments from which quantifiable results or illustrative photographs could be obtained.

Sample materials

As noted earlier, two general types of experiment were performed in this study: those aimed at establishing the principle of lithologic partitioning using well behaved but geologically unrealistic rock analogs, and those designed for direct geologic relevance but exhibiting more sluggish kinetics. For the first type of experiment, three minerals were chosen for study: quartz, calcite, and fluorite. The dihedral angles of the first two minerals in contact with aqueous fluid are well known from previous studies (Watson and Brenan 1987; Laporte and Watson 1991; Lee et al. 1991; Koga 1993; Holness 1995; Holness and Graham 1991), as is their tendency to form well-equilibrated microstructures through extensive grain growth. Perhaps equally important is the fact that their crystal structures are characterized by very different types of bonding (significantly covalent in the case of quartz and highly ionic in the case of calcite), so their interfacial structure and energetics might be expected to differ as well. Exploratory experiments revealed that fluorite also forms well-equilibrated microstructures and has a dihedral angle (against H_2O) different from both quartz and calcite.

Calcite and quartz do not coexist stably at sufficiently high P-T conditions to make these a suitable fluid partition couple, but fluorite coexists separately with both calcite and quartz at workable temperatures. Accordingly, numerous partition-couple experiments were performed using fluorite/quartz pairs and fluorite/calcite pairs; these, in fact, form the backbone of this study, because a sufficient number of experiments could be run and analyzed to establish some clear systematics.

In the results section below, some emphasis will be placed on the fact that two types of fluorite were used in both the fluorite/quartz and fluorite/calcite couples: one was reagent-grade CaF_2 containing $CaO \cdot nH_2O$ or $Ca(OH)_2$ as a significant impurity (amounting to ~1 wt% H_2O); the other was high-purity CaF_2 (Aesar Puratronic grade). The partitioning behavior of aqueous fluid is notably different in couples involving these two types of CaF_2, a phenomenon believed to result from different levels of cationic impurities in the two materials (which seem to alter the interfacial energetics significantly). In most couples involving calcite, the starting material was reagent-grade (precipitated) $CaCO_3$, although one experiment was done using natural Iceland spar ground to a grain size of ~50 μm. In most partition couples incorporating quartz, the starting material was optically clear rock crystal ground and passed through a 22 μm sieve. In a few cases, coarser quartz or silica glass were used in what turned out to be a futile effort to characterize grain-size effects on partitioning.

Aqueous fluid partition couples having more direct geologic relevance were prepared using the ground quartz (<22 μm) described above, juxtaposed against natural clinopyroxene of similar starting grain size. The clinopyroxene has a relatively Fe-rich composition lying close to the Di-Hd join but containing appreciable Mn (molecular formula $CaMg_{0.40}Fe_{0.54}Mn_{0.06}Si_2O_6$). This pyroxene was known from previous experience to coarsen more rapidly than Mg-rich compositions, thus forming much better-equilibrated microstructures (albeit ones exhibiting significant faceting). The general rationale behind the choice of pyroxene was that it might serve as a representative ferromagnesian mineral whose fluid partitioning characteristics relative to quartz could be regarded as typical of mafic vs. felsic minerals in general.

Two experiments (4 individual couples) were carried out in the peridotite/basalt system, with basaltic melt serving as the partitioned fluid (only two couples were analyzed in detail, due to concerns about equilibration of the others). The couples consisted of peridotite and harzburgite halves, varying only in their proportions of olivine and orthopyroxene—the two dominant minerals in the upper mantle. Optically clear forsteritic olivine and magnesian orthopyroxene were handpicked from disaggregated peridotite nodules (San Carlos, Arizona), ground under alcohol, and passed through a 22 μm sieve. The peridotite half of each couple contained 85 wt% olivine and 15 wt% orthopyroxene; the harzburgite half contained the same two minerals with the proportions reversed. Finely ground mid-ocean ridge basalt (MORB; 50 wt% SiO_2) was thoroughly mixed in with each mantle-analog rock at a level of 6 wt%. Each of the two experimental runs consisted of four individual samples. Two of these four were basaltic melt partition couples comprising basalt-bearing peridotite and harzburgite halves (stacking order

TABLE 1. Summary fluid partitioning experiments and results

Run no.	Couple mat'ls*	T (C)	P (GPa)	t (h)	Container†	H_2O wt%‡	ϕ/ϕ = partition coefficient§	approx. gr. dia. (μm)‖	Comments
4a	f_r/c	700	1.0	67.0	Ag	2.0+	0.113/.034 = 3.3	c:80, f:50	
4b	c/f_r	700	1.0	67.0	Ag	2.0+	0.116/.026 = 4.5	c:80, f:50	fluid segr.
5a	f_r/q	700	1.0	44.3	Ag	2.0+	0.123/.054 = 2.3	q:20, f:35	
5b	q/f_r	700	1.0	44.3	Ag	2.0+	0.083/.046 = 1.8	q:20, f:35	
6a	f_r/c	700	1.0	2.0	Pt(Ni)	2.0+	0.129/.037 = 3.5	c:20, f:15	
6b	c/f_r	700	1.0	2.0	Pt(Ni)	2.0+	0.134/.054 = 2.5	c:20, f:15	
8a	c/f_r	700	1.0	4.0	Pt(Ni)	0.5+	0.048/.009 = 5.3	c:40, f:25	
8b	c/f_r	700	1.0	4.0	Pt(Ni)	1.0+	0.073/.016 = 4.6	c:45, f:30	
8c	f_r/c	700	1.0	4.0	Pt(Ni)	2.1+	0.103/.023 = 4.4	c:35, f: 20	
9a	c/f_r	700	1.0	168.0	Pt(Ni)	0.5+	0.065/.015 = 4.4	c:120, f:80	
9b	f_r/c	700	1.0	168.0	Pt(Ni)	1.1+	0.083/.020 = 4.3	c:100, f:70	
9c	c/f_r	700	1.0	168.0	Pt(Ni)	2.1+	0.114/.034 = 3.4	c:110, f:80	
9d	f_r/c	700	1.0	168.0	Pt(Ni)	3.0+	0.134/.044 = 3.3	c:120, f:80	
10a	f_r/c	700	1.0	71.0	Pt(Ni)	0.5+	0.074/.012 = 6.1	c:100, f: 60	
10b	f_r/c	700	1.0	71.0	Pt(Ni)	1.1+	0.096/.015 = 6.6	c:100, f: 60	
10c	c/f_r	700	1.0	71.0	Pt(Ni)	2.1+	0.127/.031 = 4.2	c:80, f:50	
10d	c/f_r	700	1.0	71.0	Pt(Ni)	3.0+	0.158/.042 = 3.8	c:80, f:50	
12a	f_p/q	850	1.4	6.0	Pt(Ni)	1.0	0.042/.005 = 8.4	q:35, f:70	
12b	q/f_p	850	1.4	6.0		2.1	0.101/.008 = 12.6	q:40, f:80	fluid segr.
15c#	f_p+SiO_2 gl	850	1.4	89.0	Ag	0.5	–	q:10, f:80	
19a	q/f_p	700	1.0	139.0	Pt(Ni)	0.5	0.029/.003 = 9.7	q:30, f:80+	
19b	f_p/q	700	1.0	139.0	Pt(Ni)	1.0	0.047/.0095 = 4.9	q: 30, f:60	
19c	q/f_p	700	1.0	139.0	Pt(Ni)	2.0	0.080/.014 = 5.7	q:35, f:60	fluid segr.
19d	f_p/q	700	1.0	139.0	Pt(Ni)	3.0	0.077/.025 = 3.1	q:25, f:50	
20a	c/f_p	700	1.0	115.0	Pt(Ni)	0.5	0.018/.016 = 1.1	c:100, f:70	
20b	f_p/c	700	1.0	115.0	Pt(Ni)	1.0	0.035/.022 = 1.6	c:110, f:60	
20c	c/f_p	700	1.0	115.0	Pt(Ni)	2.0	0.066/.053 = 1.3	c:80, f:60	
20d	f_p/c	700	1.0	115.0	Pt(Ni)	3.0	0.078/.048 = 1.6	c:90, f:60	
21a	f_p/q	700	1.0	zero	Pt(Ni)	2.0	0.100/.012 = 8.3	q:5, f:5	
22a	q/f_r	700	1.0	235.5	Au(Ni)	1.0+	0.062/.0125 = 5.0	q:60, f:80	
22b	f_r/q					1.5+	na	q:60, f:80	
22c	q/f_p	700	1.0	235.5	Au(Ni)	1.5	0.082/.0134 = 6.1	q:50, f:100	fluid segr.
22d	f_p/q	700	1.0	235.5	Au(Ni)	2.0	0.109/.018 = 6.1	q:60, f:80	
23a	c/f_r	700	1.0	325.6	Au(Ni)	1.0	0.040/.033 = 1.2	c:90, f:70	
23b	f_r/c	700	1.0	325.6	Au(Ni)	1.5	0.043/.037 = 1.2	c:100, f:100	
23c	c/f_p	700	1.0	325.6	Au(Ni)	2.2	0.054/.044 = 1.2	c:80, f:80	
23d	f_p/c	700	1.0	325.6	Au(Ni)	3.0	0.077/.049 = 1.6	c:100, f:100	
26a	cpx/q	925	1.5	93.5	Ag	0.5	0.0155/.0044 = 3.5	cpx:20, q:60	
26b	q/cpx	925	1.5	93.5	Ag	2.5	0.075/.031 = 2.4	cpx:20, q:70	local melt
26c	cpx/q	925	1.5	93.5	Ag	1.2	0.051/.015 = 3.4	cpx:20, q:60	fluid segr.
27a	27c/27b	1325	1.6	138.0	C	–	see Fig. 14	ol:25, opx:15	
27b	ol+bas	1325	1.6	138.0	C	–	see Fig. 14	ol:25, opx:15	
27c	opx+bas	1325	1.6	138.0	C	–	see Fig. 14	ol:25, opx:15	
27d	27b/27c	1325	1.6	138.0	C	–	see Fig. 14	ol:25, opx:15	
28a	f_r/c	700	1.0	zero	Ag	1.1+	0.107/.00 = •	c:8, f:3	
28b	c/f_r	700	1.0	zero	Ag	2.0+	0.140/.026 = 5.4	c:8, f:4	
28c	f_p/c	700	1.0	zero	Ag	2.1	0.062/.036 = 1.7	c:8, f:5	
28d	c/f_p	700	1.0	zero	Ag	1.1	0.021/.037 = 0.6	c:7, f:6	
29a	cpx/q	925	1.5	zero	Ag	1.0	0.036/.006 = 6.0	cpx:5, q:10	
29b	q/cpx	925	1.5	zero	Ag	2.0	0.068/.036 = 1.9	cpx:8, q:8	
29c	cpx/q	925	1.5	zero	Ag	3.0	0.099/.097 = 1.0	cpx:6, q:8	
30a	c/f_p	700	1.0	44.7	Ag	3.1	0.083/.056 = 1.5	c:50, f:50	
30b	c/f_r**	700	1.0	44.7	Ag	2.1	0.054/.039 = 1.4	c:70, f:100	fluid segr.
30c	c††/f_p	700	1.0	44.7	Ag	2.1	0.080/.035 = 2.3	c:80, f:80	

* c = calcite; bas = basalt melt; cpx = clinopyroxene; f_r = reagent-grade fluorite; f_p = high-purity fluorite; ol = olivine; opx = orthopyroxene; q = quartz; SiO_2 gl = silica glass. "Numerator" denotes top position in capsule.
† C = graphite; Pt(Ni) indicates a Pt liner in an oxidized Ni cylinder (similarly for Au).
‡ Number is the amount of H_2O added to the container with a syringe at the start of the experiment; "+" refers to the additional H_2O absorbed in reagent-grade fluorite powder (see text).
§ Partition coefficients are expressed as f_{flr}/f_{cc}; f_{qtz}/f_{flr}; and f_{cpx}/f_{qtz}.
‖ These are visual estimates of average grain diameter.
Fluid localization experiment; see Figure 15.
** Pre-fired at 700 °C, 1 atm.
†† Crushed Iceland spar.

control experiments   melt partitioning couples

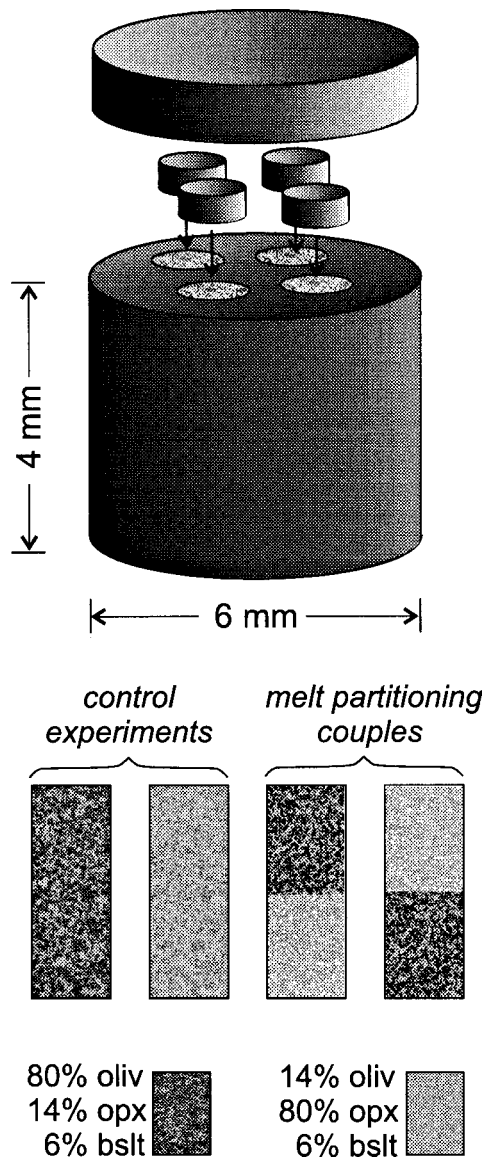80% oliv
14% opx
6% bslt

14% oliv
80% opx
6% bslt

FIGURE 4. Schematic of graphite cylinder and sample arrangement for partitioning experiments involving olivine, orthopyroxene and basaltic melts (see text).

taining isolated, ~100 μm chips of silica glass. The objective of the first two was to identify and characterize any fluid partitioning effects attributable to grain size (see theory section above), but these experiments were unsuccessful because the initial large differences in grain size were not preserved through the experiments. For a given mineral, the average grain size tends to equalize during an experiment for two reasons: first, the coarsening rate is most rapid for very small grains, so fine-grained regions "catch up" to initially coarser regions; and, secondly, extensive crushing (fragmentation) of grains occurs during initial pressurization of the samples, so powders that are relatively coarse when added to the capsules are reduced to a smaller average grain size before microstructural maturation begins. In any event, no useful information could be recovered from the experiments on quartz designed to shed light on grain-size effects.

The goal of the experiment consisting of fluorite laced with a few silica-glass chips was to produce microstructures consisting of knots of small quartz grains (crystallized from the glass) completely surrounded by polycrystalline fluorite. The idea was to see whether aqueous fluid in such an aggregate would become localized around the quartz grains, thus testing the concept of fluid partitioning on the scale of individual mineral grains (as opposed to the rock-unit scale examined in the conventional partition couples described above). These experiments were successful in that they provided some convincing photographs (see results below), but no attempt was made to recover quantitative partitioning data.

Details concerning materials used in all reported experiments are summarized in Table 1.

Experimental containers and procedures

The experiments involving aqueous fluids were performed in metal containers, of which several different types were used in an effort to optimize container design (mainly to avoid dilation cracks in the quenched samples). Simple Ag cylinders drilled with 2–4 holes to accept the partitioning couples were used in some cases. In other cases, Ni cylinders were pre-drilled, oxidized on the surfaces, and the holes subsequently fitted with Au or Pt sleeves to contain the samples (see Watson and Lupulescu 1993 for a detailed description of this technique). In all cases, closure of the containers against fluid loss was accomplished by pressure-sealing during initial sample pressurization in the piston-cylinder apparatus (see Ayers et al. 1992). The range in dimensions of the containers is indicated in Figure 3; details of containers for all experiments are included in Table 1.

The samples consisting of olivine, orthopyroxene, and basaltic melt were contained in graphite cylinders drilled to accept four individual samples in the same manner as used for the aqueous fluid-bearing runs (Fig. 4).

The procedures used in the preparation and execution of the experiments were similar for all samples and containers. In the case of the aqueous fluid partition couples, the powders were packed into their containers with a metal tamping tool and the total masses of material recorded for subsequent calculation of the amounts of H_2O needed for the desired overall fluid fractions. Distilled H_2O was added with a microsyringe

reversed in the two couples); the other two were separate control samples of peridotite and harzburgite, each containing 6 wt% basalt (see Fig. 4), which were included to provide information on the inherent melt content of these two systems when they were equilibrated independently at run conditions.

In addition to the materials and sample geometries described above, a few experiments were conducted using other materials and/or physical arrangements. These included: (1) partition couples comprising separate halves or alternating layers of fine and coarse quartz; (2) couples consisting of quartz powder in one half and ground silica glass in the other; and (3) a sample composed dominantly of fluorite (initially <22 μm) but con-

just prior to assembling and pressurizing the piston-cylinder cell (thus minimizing H_2O loss through evaporation). The samples were first cold-pressurized to a value exceeding the desired run pressure by ~20%; they were then heated at 75 °C/minute and stabilized at the final run temperature. Manual pressure adjustments were made over the first few hours of the run to counteract relaxation of the assembly. Temperature was monitored and controlled with $W_3Re_{97}/W_{25}Re_{75}$ or chromel/alumel thermocouples to within 1–2 °C; the overall temperature uncertainty is believed to be within 10 °C of the nominal (reported) values. As noted earlier, some temperature gradients are expected along the sample container in any piston-cylinder assembly. For the Ag (and probably the Ni) sample containers, these gradients are small (see Fig. 4 of Watson and Wark 1997), amounting to no more than 10 °C variation for the largest capsules. As a precaution, the samples in experiments numbered 22 and higher were downsized to 3–4 mm in length from the 5–6 mm of most earlier runs. In the one basaltic melt partitioning experiment for which data are reported (no. 27; conducted in graphite) the samples were only about 2 mm long.

Experiments were terminated by cutting off the power to the graphite heater of the piston-cylinder assembly, which resulted in cooling below 100 °C within a few seconds. No attempt was made to maintain constant pressure during the quench, and pressures typically dropped to 50–60% of run-condition values as room temperature was approached. The metal or graphite cylinders were recovered from the piston-cylinder assembly, cut and ground to obtain near-axial sections of all samples, and polished to 0.3 μm alumina for electron microscopy and image analysis.

The three partitioning runs reported in Table 1 as zero-time experiments were prepared in exactly the same manner as the long-duration runs, but they were terminated as soon as run conditions were reached. In other words, the capsules were loaded, pressurized, ramped up to a pre-determined temperature at 75 °C/minute, and quenched immediately upon reaching that temperature. The purpose of these runs was to assess the distribution of fluids in the couples at the initiation of partitioning experiments, in order to confirm that the results are independent of possible mechanical effects taking place during cold pressurization of the powders. This was a particular concern in the case of the fluorite/quartz couples because quartz is far stronger than fluorite: cold pressurization of the stacked powders could simply squeeze the water out of the weak fluorite and into void space held open by the strong quartz grains.

Analysis

The main type of analysis conducted on the synthetic, porous rocks was porosity determination of the two halves of the quenched partition couples. The porosity was assumed to represent the volumetric fraction, ϕ, of fluid present at run conditions (the molar volume of aqueous fluid at the experimental conditions is close to that at room conditions, so there is little tendency for collapse or expansion of the pores during quenching and decompression). Digital images of the sectioned and polished couples were acquired with a scanning electron microscope (SEM), using backscattered electrons (BSE) in most cases (secondary electrons were used for a few samples). The entire couple

was first imaged at ~40× to obtain a map. Detailed, representative images of each half were then acquired at magnifications varying between 150× and 10,000×, depending upon the grain- and pore size of the sample (a magnification of 300–600× was typical). The frames were selected to represent a significant fraction of the polished area of each rock, including as much of the axial length (i.e., distance above and below the interface) as possible. The digital images (~1 Mbyte each) were imported into an image analysis program (SigmaScan Pro 4.0) for determination of pore area fractions. Thresholding of the grayscale for automated discrimination of features was usually straightforward, because the pores generally appear black against light-gray minerals. However, the polished surfaces of many samples had imperfections, including plucked grains and dilation cracks perpendicular to the axis of the cylindrical couples (such cracks are common in samples recovered from solid-media pressure apparati, because uniaxial unloading is done during or after the thermal quench). For this reason, manual editing of most images was required in order to exclude cracks and other surface imperfections. Familiarity with the typical shapes of pore features in equilibrated microstructures made this time-consuming process relatively straightforward in most cases, if not totally objective. In terms of both thresholding and coping with imperfections during image analysis, the zero-time experiments presented the greatest difficulties, due to the small size and irregular shapes of grains and pores.

The samples containing basaltic melt presented the greatest difficulties in image analysis for melt fractions, because the melt pockets quenched to a mixture of glass, clinopyroxene crystals, overgrowth rims on existing olivine and orthopyroxene, and occasional exolved bubbles (the 19 mm piston-cylinder assemblies used in this study do not cool as rapidly as the 12.7 mm assemblies used in other studies of molten peridotite textures). Efforts were made at automated determination of areas of all phases in the digital images, but in the end it was necessary to simply trace out the quenched melt pools manually on the computer screen.

Dihedral angles (θ) were measured for several fluorite and calcite samples and one quartzite (see Table 2). The measurements were made by visually estimating (on the computer screen) tangents to the two curved crystal/fluid interfaces where they intersect a grain boundary, and calculating the angle between them (see Fig. 1b). The usefulness of the resulting data for predicting or interpreting fluid partitioning tendencies is limited for reasons discussed in the theory section. However, observed differences in θ for a particular mineral in different partition couples can be used to rationalize observed partitioning differences, and to demonstrate that θ for a given mineral depends upon the nature of the solutes present in the fluid. The single-operator reproducibility of θ values measured on a single image is within 2 to 3°, depending on the number of measurable angles in the image (~80 to 500 were measured in each case; see Table 2).

At the outset of this study, it was anticipated that fluid partitioning might be sensitive to grain size (see theory section) so detailed grain-size characterization of the samples was planned. It quickly became clear, however, that for partition couples involving two specific rock types, the partitioning behavior did

TABLE 2. Summary of q measurements on selected samples

Expt.	Frame*	Mineral†	q	n‡	Comments
5a	1	f_r	48	390	
5b	1	f_r	48	380	
10c	4			68	500
10b	1	f_r	68	450	
19b	5	f_p	63	108	close to qtz
19b	6	f_p	76	78	
19b	7	f_p	61	192	
19b	10	f_p	59	201	far from qtz
19c	4	f_p	63	152	close to qtz
19c	5	f_p	72	78	
19c	6	f_p	71	106	
19c	7	f_p	73	103	
19c	8	f_p	72	86	far from qtz
19d	6	f_p	54	140	close to qtz
19d	7	f_p	53	193	
19d	8	f_p	52	264	
19d	9	f_p	53	144	far from qtz
20d	1	f_p	70	330	
20d	4	c	64	250	
22a	3	q	46	296	
22b	3	f_r	66	457	
22d	3	f_p	63	288	
23d	1	f_p	79	504	

* Specific image in sample (see, e.g., Fig. 5, 8, and 10).
† Symbols as in Table 1.
‡ Number of apparent angles measured.

not change measurably over large variations in grain size (~15–100 μm). Accordingly, only qualitative estimates of grain size are included in Table 1.

Concerns and complications

In this study, even a well-executed and accurately characterized experiment is subject to possible uncertainty in significance and interpretation. Some reasons for caution were already noted in the description of the methodology, but it may be useful to summarize and augment the list of concerns—and how they were addressed—before proceeding to the results. They are:

(1) *The possible influence of a temperature gradient* in determining the final distribution of fluid in a partitioning experiment. This possibility was ruled out by showing that partitioning behavior was independent of the relative position (top vs. bottom) of the two synthetic rock types [the thermal profile in the piston-cylinder assembly is not symmetric along the capsule axis; see Watson and Wark (1997)].

(2) *Mechanical effects during cold compaction of the couples.* These were addressed by performing zero-time experiments and comparing the resulting fluid distribution with that of much longer experiments.

(3) *Incomplete connectivity of aqueous fluid* in polycrystalline calcite and fluorite as a consequence of the high dihedral angle (see von Bargen and Waff 1986). Connectivity of fluid in calcite has been shown to be established at $\phi \sim 0.015$ (Wark and Watson 1998); similar behavior is expected in fluorite because of the similarity in θ of the two materials. In many partitioning

experiments, ϕ in both rocks was higher than 0.015, so there is no doubt that extensive connectivity of fluid was achieved in these cases. In those instances where ϕ was less than 0.015 in one half of the couple, the partitioning results are consistent with higher-ϕ experiments.

(4) *Segregation of fluid into large pockets.* In some cases, it may be energetically favorable (or kinetically expedient) for fluid to segregate into large pools or pockets rather than remain uniformly dispersed on the scale of individual grains in each rock. Such segregation is not unexpected [see theory section and Watson and Brenan (1987)] and was in fact observed in some cases and inferred in others (see discussion below). The presence of a large fluid segregation in a sample does not invalidate partitioning information obtained from measurement of the dispersed porosity remaining in the two rocks.

(5) Theoretically, a *difference in grain size* of the two halves of a partition couple can play a role in fluid partitioning. Because the grain sizes of the two rocks in a partition couple were never exactly the same, the superimposition of grain-size effects upon mineralogical effects cannot be ruled out. The grain sizes of calcite and fluorite are, however, quite similar (see Table 1), so any grain-size effect on fluorite/calcite partitioning is likely to be small. In other types of partition couples (fluorite/quartz and clinopyroxene/quartz), differences in grain size are substantial—and the fluid is partitioned into the finer-grained
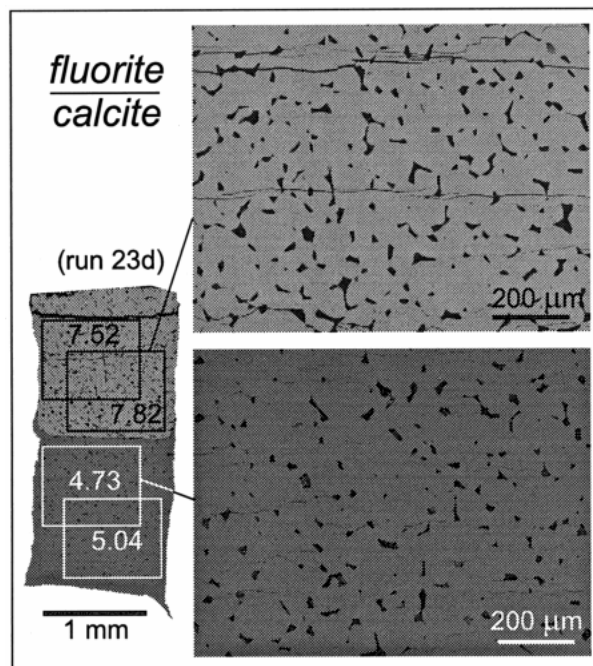

FIGURE 5. BSE images of sectioned fluorite/calcite fluid partitioning couple run at 700 °C and 1 GPa for 326 h (run no. 23d). At left is the entire couple, showing locations of higher-magnification frames taken for image analysis. The two shades of gray are fluorite (lighter, top half) and calcite (darker, bottom half). The black features are pores (occupied by fluid at run conditions). The horizontal black lines are dilation cracks produced during cold decompression of the sample; these were edited out during image analysis to obtain the pore percentages ($\phi \times 100$) indicated by the small numbers on the figure.

rock in both cases. Grain size differential may be a factor in these cases, but its influence on fluid partitioning cannot be separated from that of intrinsic interfacial energy differences or faceting.

RESULTS

Calcite/fluorite partitioning of H_2O

All data reported for the system calcite (cc) + fluorite (flr) were obtained from partition couples run at 700 °C and 1.0 GPa. As previously noted, some of these couples incorporated reagent-grade CaF_2 (containing CaO and H_2O as impurities), others involved high-purity CaF_2. The experiments ranged from 0 to 326 hours in duration, and yielded a wide range of sample grain sizes: ~5 μm for a zero-time experiment, ~15–20 μm in 4 hours (run no. 6), and ~100 μm in 326 hours (run no. 23). A typical calcite/fluorite run product is shown in Figure 5.

The zero-time experiment (no. 28, containing 4 individual couples) is of critical significance because it establishes the distribution of fluid at the start of the partitioning process. Backscattered-electron images of two couples from this experiment are shown in Figure 6. Figure 6a contains high-magnifi-

cation images from couple 28a, which consisted of calcite (bottom) and reagent-grade fluorite. The images reveal that essentially all the fluid in this couple is localized in the fluorite half. In the calcite half there was unavoidable plucking of grains during sample polishing, but it is clear nevertheless that the visible grain edges contain little or no fluid. The fluorite, in contrast, has an average measured porosity of ~10.7 vol%, which is equal to the fluid added as liquid H_2O (~3.6 vol% overall, or ~7.2 vol% of the fluorite alone) plus that initially contained as adsorbed H_2O in the reagent CaF_2 (~3.4 vol% of the fluorite at run conditions). It is not obvious why virtually all the fluid should be contained within the fluorite in the zero-time experiment using reagent-grade material, but the explanation may lie in the fact that the reagent fluorite is an extremely fine, fluffy powder that absorbs all added water prior to pressurization of the couple. In any event, this initial distribution is significantly different from that obtained in runs of any duration, which indicates that re-distribution of fluid occurs during microstructural maturation.

Figure 6b (couple 28d) shows a very different zero-time distribution of fluid when high-purity fluorite (passed through a 22 μm sieve) is placed against calcite. The same amount of
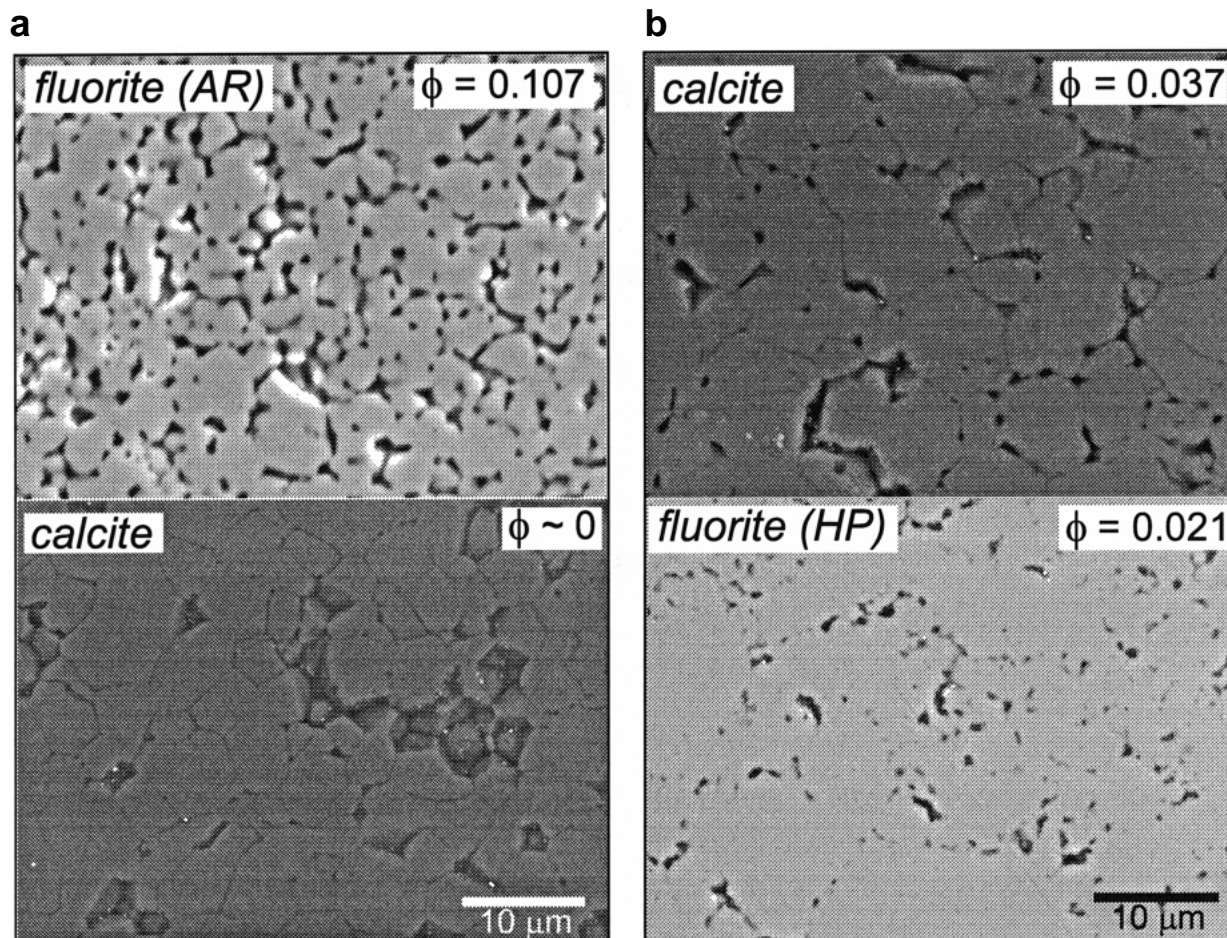
a

b

FIGURE 6. BSE images of zero-time calcite/fluorite fluid partition couples with ~1 wt% added H_2O (run nos. 28a and 28d). (**a**) Couple containing analytical reagent (AR) grade fluorite (with adsorbed H_2O); (**b**) couple containing high-purity fluorite. Note the differences in the initial distribution of the porosity in the two couples; see text for discussion.

liquid H_2O was added to this couple as for 28a (see Table 1), but in this case no additional moisture was contained in the fluorite itself. The images reveal that in this case there is actually more fluid in the calcite than in the fluorite. Also in contrast with couple 28a is the fact that fluorite shows no perceptible recrystallization and the calcite grains are larger (both these observations are consistent with the very different initial distribution of H_2O). The one respect in which 28a and 28d are alike is that both show fluid distributions significantly different from those established in longer runs. In couple 28d, in fact, the sense of the partitioning is opposite to that produced in longer runs. This is taken as a clear demonstration that the final distribution of fluid (i.e., that measured in long experiments) is not attributable to mechanical or other effects occurring during run-up of the experiments.

The results of 28 calcite/fluorite partitioning experiments are summarized in Figure 7, which is a plot of the measured vol% of fluid (i.e., $\phi \times 100$) in the calcite and fluorite halves of the couples against the total amount of fluid in the system. It is immediately clear from this figure not only that the overall partitioning is strongly systematic, but also that the results for the reagent-grade fluorite are markedly different from those for the high-purity fluorite. The direction of fluid partitioning is the same (ϕ is higher in the fluorite), but the partitioning effect is much stronger in couples containing reagent CaF_2 (three- to sixfold enrichment) compared with couples containing high-purity CaF_2 (enrichment by a factor of 1.3 to 1.6). The specific cause of this difference is unclear, but two possibilities can be identified: differing levels of cation impurities (which could cause differences in interface energetics), or differences in pH of the aqueous fluid. Dihedral-angle measurements were made on both types of fluorite in calcite/fluorite couples: $\theta = 70°$ and $79°$ for high-purity fluorite in two different couples; $\theta = 68°$ for reagent-grade fluorite in one couple (see Table 2). Considering the uncertainty in θ measurements, the $79°$ value is the only one that can be regarded as different from the others. Even if the θ values for the two fluorites really do differ from one another, θ values alone do not predict fluid partitioning behavior (see theory section). Observed differences in θ do, however, hint at possible underlying differences in interface energetics of the two materials, which could indeed cause differences in fluid partitioning.

One calcite/fluorite partition couple (no. 30b; gray symbol in Fig. 7) was prepared using the reagent-grade fluorite that had been devolatilized in air at 700 °C prior to loading into the container. Curiously, the observed partitioning behavior is intermediate between those of the high-purity and untreated reagent-grade fluorites. This would seem to suggest that the overall difference in fluid partitioning between calcite and the two fluorites is due at least in part to a volatile component in the reagent-grade material.

Leaving aside the differences in aqueous fluid partitioning attributable to the level of impurities in the fluorite, the systematics revealed in Figure 7 are impressive. It is clear, for example, that a linear fit to the data for reagent-grade fluorite would pass close to the origin of the plot—a behavior reminiscent of trace-element partitioning between coexisting phases. The same does not appear to be true of the fluid abundances in
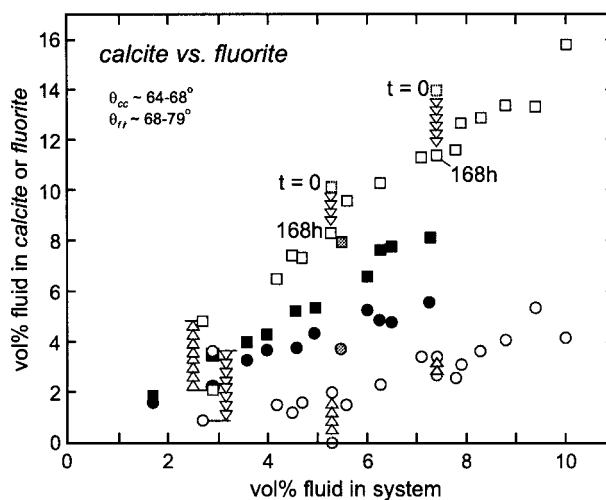

FIGURE 7. Summary of aqueous fluid partitioning results for the calcite-fluorite system, emphasizing the difference in partitioning behavior between couples containing high-purity fluorite (black symbols) and reagent-grade fluorite (open symbols). In all cases, the squares represent fluorite and the circles calcite; coexisting fluorite-calcite pairs in individual experiments are vertically aligned. The gray symbols represent a single experiment containing pre-fired reagent-grade fluorite. Three of the long-duration experiments have zero-time equivalents (dotted-outline symbols); the progression from zero-time to the long duration result is indicated by the extended arrows. All runs were made at 700 °C and 1 GPa, for durations ranging between zero and 326 hours. The average grain size of fluorite and calcite (excluding zero-time runs) ranges from ~20 to ~100 μm (see text and Tables 1 and 2).

the calcites paired with these samples: a linear fit to these data would intersect the x axis of the plot. Alternatively, the calcite data could be fit to a concave-upward function that does pass through the origin. In either case, the partitioning ratio (ϕ_{fir}/ϕ_{cc}) for these impure couples varies with the changes in the amount of fluid in the system: at low fluid abundances ($\phi < 4$ vol% overall), the ratio is about 6, but it drops to about 3 for the most fluid-rich couples (~10 vol% fluid). Data from the couples containing high-purity fluorite appear to define linear arrays that would pass close to the origin if extended to lower fluid abundances. No actual fits are shown on the diagram because there is no theoretical expectation of any particular functional dependence (see theory section).

Quartz/fluorite partitioning of H_2O

Most of the fluorite/quartz couples that yielded partitioning data were run at 700 °C and 1 GPa, although two values were also obtained from experiments at 850 °C and 1.4 GPa. As in the calcite/fluorite experiments, both reagent-grade and high-purity fluorite were juxtaposed against quartz. The experiments varied in duration up to 236 hours, and yielded average grain sizes ranging from ~20 to 50 μm for the quartz and ~50 to 100 μm for the fluorite (a zero-time experiment produced average grain sizes ≤10 μm for both phases). Fluorite coarsens more rapidly than quartz, so the average fluorite grain size was con-
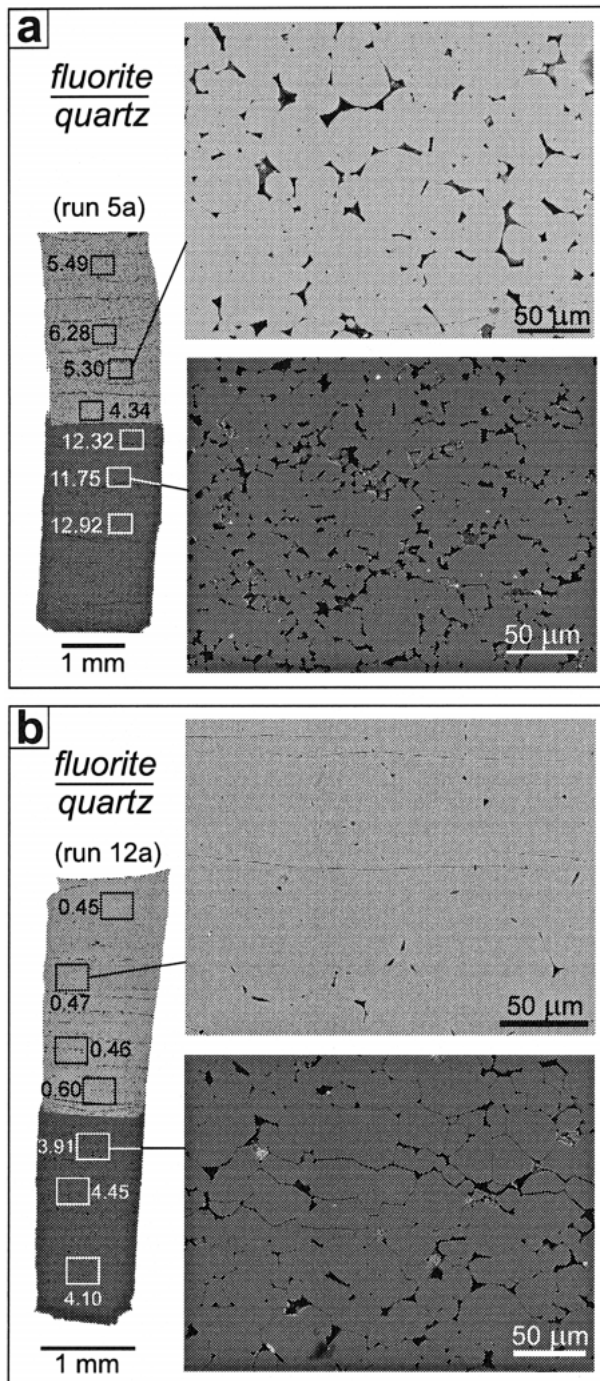
FIGURE 8. BSE images of the polished surfaces of two fluorite/quartz partition couples; arrangement and annotation similar to that in Figure 5. The lighter-gray phase is fluorite, the darker is quartz; black regions are pores; bright spots are blebs of noble metal and impacted polishing compound. In **a** (run no. 5a: 700 °C, 1 GPa) the fluid is partitioned into the quartz by a factor of ~2. In **b** (run no. 12a: 850 °C, 1.4 GPa) the partitioning is considerably stronger (note pore percentages on figure).

sistently about twice that of quartz. This grain-size mismatch contrasts with the fluorite/calcite couples, in which the grain sizes of the two phases were subequal (calcite always slightly larger). Another difference between the quartz/fluorite and calcite/fluorite couples is that quartz exhibits significant faceting, which is rarely observed in calcite and fluorite. BSE images of typical quartz/fluorite partition couples are shown in Figure 8.

Prior to describing the quartz/fluorite partitioning results, it is important to note that the dihedral angle for fluorite against aqueous fluid (θ_{flr}) shows significant variability in the quartz/fluorite couples. A value of 60–65° is typical, which is somewhat lower than for fluorite in a quartz-free system—probably because silica is soluble in the fluid and alters the chemistry of the fluorite/fluid interface. The lowest value (48°) was measured for reagent-grade fluorite in the two couples of run no. 5 (see Table 2); however, this low value is neither characteristic of nor restricted to the reagent-grade fluorite. In run no. 22b, for example—which involved reagent-grade material—θ_{flr} is 66°. The only difference between run nos. 5 and 22b is that no. 5 was run in Ag and no. 22 was run in Au. Adding to the complexity is the fact that one partition couple incorporating high-purity fluorite (no. 19d, contained in Pt) also exhibits a low θ value of 53°, demonstrating that low values are not restricted to fluorite containing significant impurities.

Figure 9 is a summary of aqueous fluid partitioning between quartz and fluorite. As in the case of calcite/fluorite partitioning, there is significant enrichment of fluid in one half of the couples—in this case the quartzite. Two aspects of the data set are noteworthy: (1) the strong overall systematics (a regular increase in ϕ of both rocks with increasing abundance of fluid in the system); and (2) an apparent correlation between θ_{flr} and
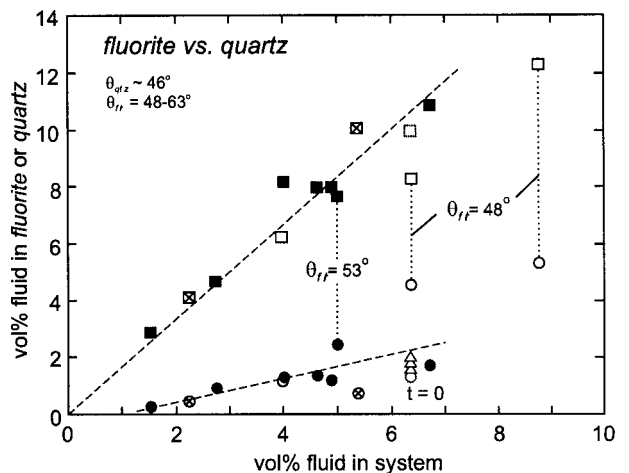

FIGURE 9. Summary of aqueous fluid partitioning results for the fluorite-quartz system, arranged as in Figure 7. Black symbols represent partition couples containing high-purity fluorite run at 700 °C, 1 GPa; open symbols show results for couples run at the same conditions containing reagent-grade fluorite (squares are quartz and circles fluorite; coexisting pairs are aligned vertically). Symbols with ×s show results of runs made at 850 °C and 1.4 GPa; the dotted symbols represent a single zero-time partition couple. See text for discussion and tables 1 and 2 for experiment details.

the strength of partitioning into the quartzite. In reference to the latter point, note that the three samples exhibiting lower θ_{flr} values (53, 48, and 48°; see Fig. 9) also show weaker partitioning of fluid into the quartzite, and the fractionation is weakest when $\theta_{flr} = 48°$. Samples exhibiting θ_{flr} of 60–65° appear to define a single trend (though slightly stronger fractionation is suggested at 850 than at 700 °C where most experiments were done). The quartz/fluorite zero-time experiment is not definitive in the sense that it shows apparent partitioning behavior indistinguishable from the typical-θ_{flr} data. For these particular experiments, then, the main evidence for equilibration is that there is no apparent dependence of partitioning behavior upon experiment duration. Moreover, the system *does* respond to changes in θ_{flr}.

Clinopyroxene/quartz partitioning of H_2O

Information on partitioning of aqueous fluid between clinopyroxenite and quartzite was obtained from three couples (experiment no. 26) run at 925 °C and 1.5 GPa for ~94 hours. For comparison, a zero-time experiment was made at the same conditions. Figure 10 is a BSE image of the couple containing ~4 vol% total fluid (26c). The image reveals a significant difference in average grain size between the two: ~15 μm for the pyroxenite and ~60 μm for the quartzite. Other features include a large fluid segregation at the interface between the two rocks and extensive faceting of the pyroxene grains. BSE images of one of the zero-time couples (no. 29c; Fig. 11) reveal similarity in initial grain sizes and extensive crushing of pyroxene and quartz grains upon cold pressurization.

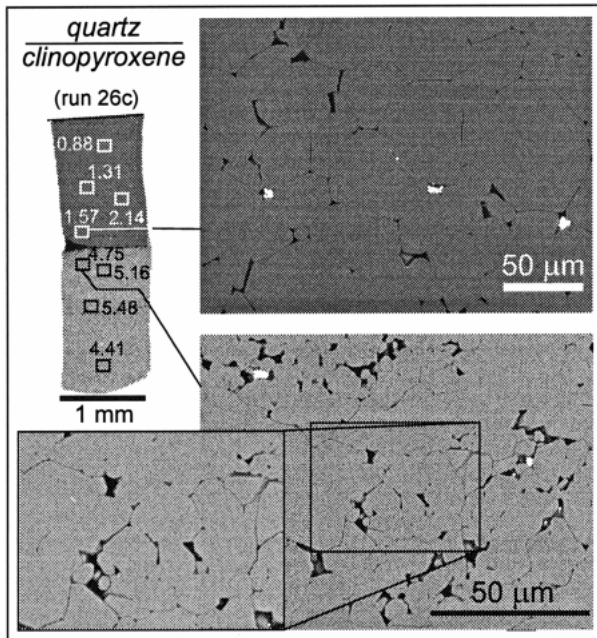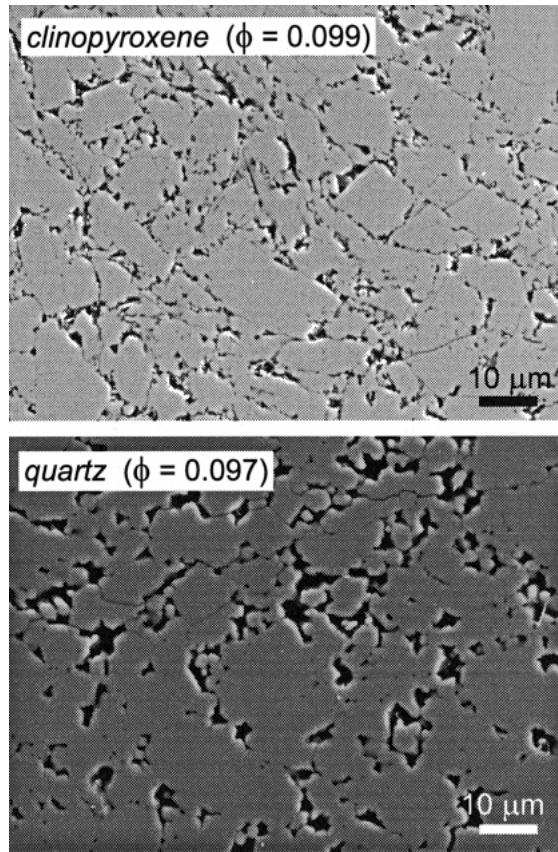The partitioning results are summarized in Figure 12 as a

FIGURE 11. High-magnification images of the polished surface of zero-time aqueous fluid partition couple (no. 29c) containing clinopyroxene (top frame) and quartz (bottom frame). Note the angular grain fragments and near-equal distribution of fluid. See text and Figure 12.

FIGURE 10. BSE images of the polished surface of a quartz-clinopyroxene aqueous fluid partition couple (run no. 26c: 925 °C, 1.5 GPa). Dark gray is quartz; lighter shade is clinopyroxene; bright blebs are Ag metal. Annotation similar to Figures 5 and 8.
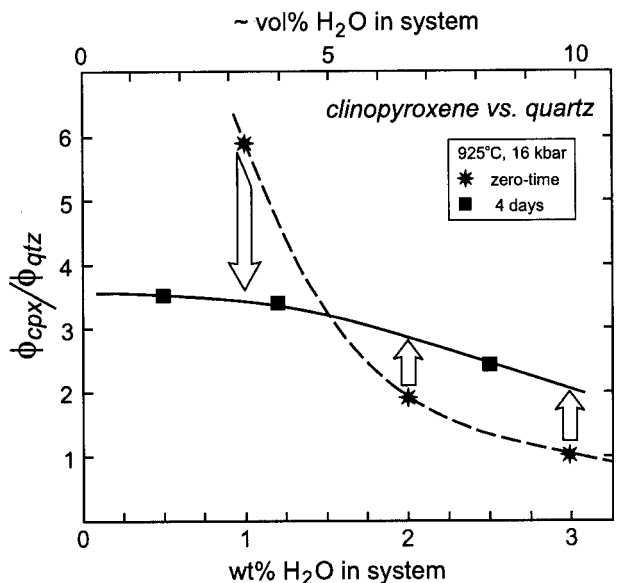

FIGURE 12. Summary of aqueous fluid partitioning results for the clinopyroxene-quartz system, comparing zero-time and 4-day experiments.

plot of ϕ_{cpx}/ϕ_{qtz} vs. the total amount of fluid in the system. This diagram differs slightly from the fluid-distribution diagrams shown previously (Figs. 7 and 9) to facilitate comparison of the zero-time and long-duration results. It appears from the zero-time couples that small amounts of fluid are initially localized in the pyroxenite, but under more fluid-rich circumstances the initial distribution approaches uniformity: $\phi_{cpx}/\phi_{qtz} \approx 1$ at ~10 vol% bulk fluid. These zero-time results contrast sharply with the distribution of fluid observed after ~94 hours, when $\phi_{cpx}/\phi_{qtz} \approx 3.0 \pm 0.5$ in all three couples (see Fig. 12).

Peridotite/orthopyroxenite partitioning of basaltic melt

One set of "upper mantle" partition couples (run no. 27) was analyzed in detail by manually tracing around the quenched melt pockets (see analysis section). The results do not lend themselves to graphical treatment, and are presented as simple maps of the two partition couples and control samples (Figs. 13 and 14). Local melt percentages are indicated for several ~130 × 180 μm regions across each sample. Plausible melt percentages were obtained for the samples (averaging 6.1 vol% —roughly the amount of MORB added to the olivine + orthopyroxene mixtures), but there are no statistically significant differences in melt abundance between the halves of the two couples. Thus, either the surface energetics of olivine and orthopyroxene are very similar (so there is little tendency for melt fractionation between the dunite and the pyroxenite), or the ~6 day duration was insufficient for measurable redistribution of melt.

Grain-scale localization of aqueous fluid

The results of the fluid localization experiment (no. 17a) are conveyed most easily with BSE images, four of which are shown in Figure 15. Each image is centered on a knot (≤100 μm in size) of tiny quartz grains that is completely surrounded by much larger grains of fluorite. The total porosity of the sample is only about 1.6 vol% (based on the amount of H_2O added at the outset) and ϕ_{flr} is exceedingly small. The fluid has become highly localized within and around the quartz knots, giving them a much higher porosity than the rest of the sample. Inasmuch as these knots were formed by gradual crystallization of large silica glass chips initially dispersed through the sample, there is no question here of any mechanical injection of H_2O into the polycrystalline quartz knots during cold pressurization of the sample. Note also that many of the triple junctions (grain edges) in the fluorite appear to be completely devoid of fluid (at least four dry grain edges appear in the lower right panel of the figure).

DISCUSSION

Mechanisms of fluid re-distribution

Up to this point, a key question that has been left unaddressed is the mechanism(s) by which fluid in a system redistributes itself to achieve an equilibrium partitioning between or among lithologic units. Imagine a simple system consisting of only a large fluid reservoir in contact with a single rock type (Fig. 16). If the porosity of the rock is lower than the minimum-energy fluid fraction ϕ_m, then fluid must infiltrate the rock in order to minimize the energy of the system (Fig. 16a). The
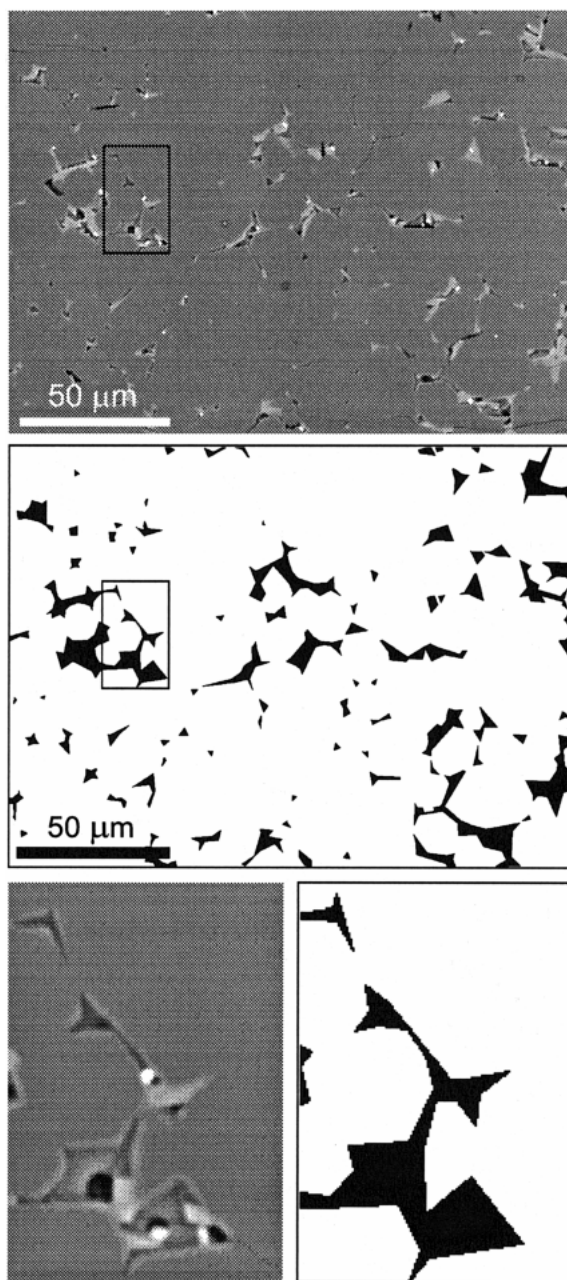

FIGURE 13. Illustration of sample characteristics and image analysis technique for melt partition experiments containing olivine, orthopyroxene, and basalt. The top panel is a representative BSE image of a polished sample surface. The medium-gray regions are olivine or orthopyroxene (these are indistinguishable at the contrast setting used); the lighter-gray regions consist of glass and quench pyroxene and olivine; the dark spots are graphite crystals and vapor bubbles (the latter were produced during quench); the localized bight spots are chromite. The image analysis involved manually tracing the inferred boundaries of the melt pools present at run conditions to produce a black and white bitmap like that shown in the middle panel (see text). The rectangular area is enlarged in the bottom panel as both a grayscale image (left) and corresponding black and white bitmap. The melt pool margins at run conditions were considered to be the inner boundaries of the quench growth.

system is presumed to be in mechanical equilibrium, so it is not a matter of injecting overpressurized fluid to open up the grain boundaries of the rock. Rather, the fluid becomes redistributed through a process of grain dissolution within the rock (enlargement of pores) balanced by precipitation within the reservoir to maintain chemical equilibrium in the system. Precipitation involves either addition of material to the grains at the reservoir/rock interface or nucleation of new grains near the interface (Fig. 16a; see also Nakamura and Watson 1999). If the fluid phase is interconnected (i.e., $\theta \leq 60°$), then the transfer of material out of the rock can occur by solute diffusion in the fluid (or, more specifically, by interdiffusion of the mineral components with the other components of the fluid), which rate-limits the overall infiltration process. Infiltration results in an increase in the volume of the porous rock (i.e., crystals + pores) and advancement of the reservoir/rock interface into the reservoir.

Figure 16b illustrates the opposite case in which the rock contains more fluid than required for minimum interfacial energy of the system ($\phi > \phi_m$; θ still $<60°$). Under these circumstances the rock expels fluid, and the mechanism is simply the reverse of that described above: dissolution of mineral grains at the reservoir/rock interface with mass-balancing precipitation within the pores, the latter reducing ϕ toward ϕ_m. The processes of dissolution and precipitation are again coupled by diffusion through the interconnected fluid.

The additional case involving a fluid reservoir adjacent to a rock whose grain edges are not wet by the fluid (i.e., $\theta > 60°$) must be addressed before turning to partition couples. From Figure 1 it is that clear that—at least for the idealized systems represented—the minimum-energy fluid fraction still applies to non-wetting fluids if $60° < \theta < 75°$. Given a fluid reservoir adjacent to such a rock (Fig. 16c), the overall system is at a minimum energy if ϕ_m is achieved within the rock, as was the case for interconnected fluid. Simultaneous dissolution and precipitation are still plausible mechanisms for redistributing mass, but they can no longer be coupled by diffusion through
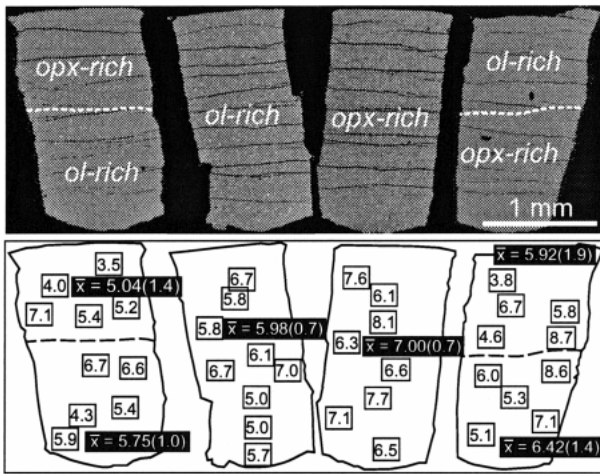

Figure 14. (**Top**) low-magnification BSE images of sectioned samples from run no. 27. (**Bottom**) results of image analysis for melt percentages present at run conditions (see text, Figs. 4 and 13).

FIGURE 15. BSE images of polished surface of run no. 15c showing knots of small quartz grains (dark gray) imbedded in a matrix of much larger fluorite grains (light gray). Note the localization of porosity (black) in and around the clusters of quartz grains. The black arrows indicate fluorite grain triple junctions that are devoid of fluid. The total fluid content of the capsule was 0.5 wt%. See text for discussion.
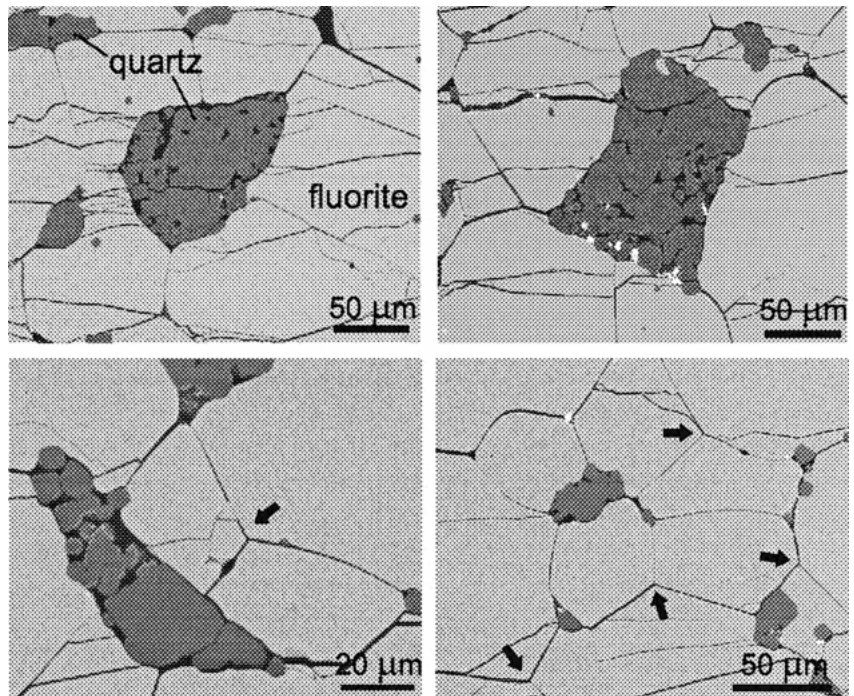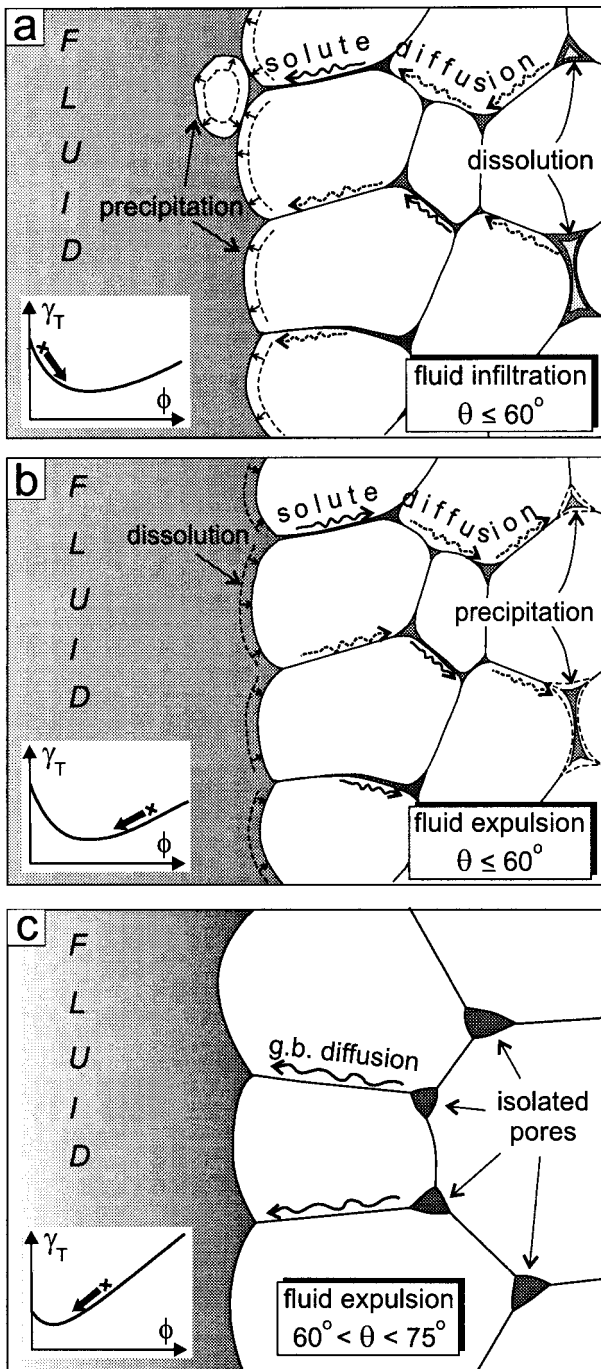
FIGURE 16. Schematic representation of the interaction between a fluid reservoir and a fluid-bearing rock that is close to microstructural equilibrium. (**a** and **b**) Illustrative of cases in which the fluid is interconnected and ϕ is either below or above ϕ_m, leading to either infiltration (as in **a**) or expulsion (as in **b**) of fluid from the rock. In **c** the fluid-filled porosity is not interconnected. See text for further explanation.

interconnected fluid. Instead, communication between the fluid reservoir and the pores of the rock must occur by molecular diffusion of the fluid components along the grain boundaries of the rock. This distinction is seen as important because grain-boundary diffusion is almost certainly much less efficient at redistributing fluid than is diffusion through interconnected fluid.

Fluid segregation in partition couples

The foregoing discussion provides a good basis for interpreting the presence of large, segregated pockets of fluid at the interface between the two rock types in several partition couples (see Table 1). Included in the table are a few high-ϕ experiments in which segregations are not actually observed at the polished surface but whose presence is implied by the fact that the fluid added at the start is not fully accounted for in the post-experiment image analyses. Images of incipient to fully developed segregations are shown in Figure 17. These features were present at run conditions—i.e., they are not pull-apart or differential shrinkage/expansion features formed during quench. This is clear because they terminate at the capsule wall or within the sample itself, and because they contain quenched solute in general proportion to the size of the segregation (see Figs. 17a–c). Because of the low solute content of the fluid, a relatively large fluid volume is required to produce enough quench solute in a localized area to be visible in polished section (quenched solute is never observed in ordinary pores at the SEM magnifications used in this study).

Why do these segregations occur? The key to the answer is that they are invariably located exactly at the interface between the two rocks, which proves that they are not related to small temperature gradients that might exist along the couples (conceivably, fluid could become concentrated at the hottest point along a capsule, but there is no reason why this point should coincide exactly, in every case, with the lithologic interface). Two plausible explanations remain: (1) there is sufficient fluid in the system to exceed ϕ_m in both rocks, so γ_T is minimized by segregation of fluid; or (2) fluid is expelled from one rock faster than it can infiltrate the other. Despite the appeal of the first hypothesis, the second one is favored as the correct one. The first hypothesis does not explain why segregations occur in samples other than those with the highest overall ϕ (even though they are never observed in the lowest-ϕ samples). Moreover, like the temperature-gradient hypothesis, it does not explain why the segregations occur exactly at the interface between the two lithologies. The segregations seem to be particularly common in the quartz/fluorite couples. Recall that, because of the mechanics of cold compression of these couples, almost all the fluid is initially located in the quartzite. At run conditions, the high degree of fluid interconnectivity in this low-θ rock may result in rapid expulsion of fluid from the quartzite at a rate that cannot be matched by uptake of fluid into the higher-θ fluorite (see Fig. 16). The only unsatisfying aspect of this interpretation is that the segregations become transient features. This is difficult to reconcile with the general consistency in lithologic partitioning behavior of fluids in all couples of the same phases, which is readily apparent from the strong systematics of the data shown in Figures 7 and 9 (which include couples with and without segregations).
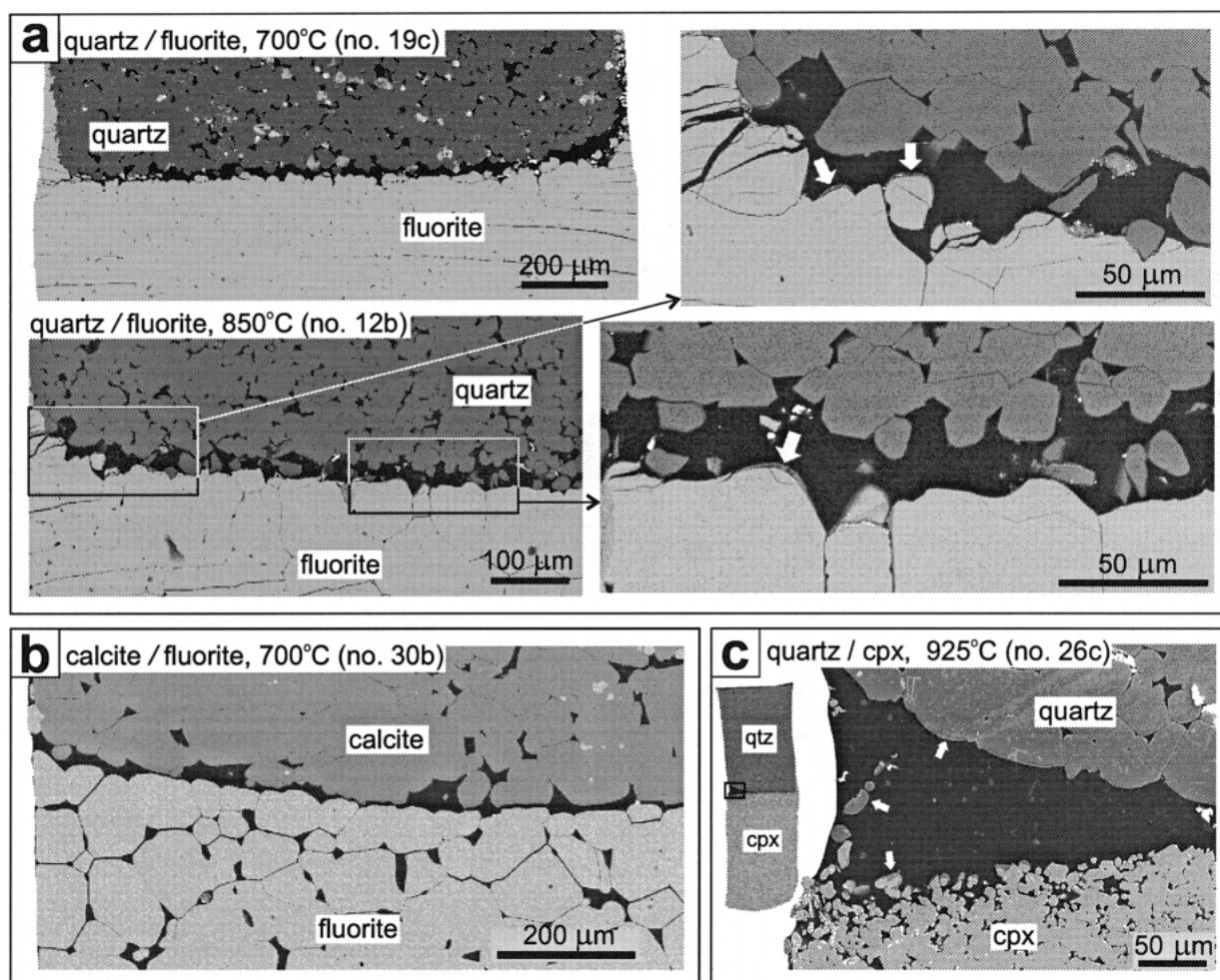
FIGURE 17. BSE images of polished fluid-partition couples showing several examples of fluid segregation at the interface between the two rock types. (**a**) The boundary regions of two quartz-fluorite couples are shown, with enlargements of key areas showing quenched solute (white arrows). (**b**) Incipient segregation at a calcite-fluorite boundary. (**c**) A large fluid pocket at the interface between quartzite and clinopyroxenite (white arrows point to quenched solute). The bright pore-filling material (especially apparent in the quartzite of run 19c in a is mostly impacted polishing compound; occasional Ag blebs are also visible. See text for discussion

Geologic implications and future directions

The firmest conclusion of this study is that fluid localization—both within specific lithologic units and around certain minerals—can be expected in geologic systems as a consequence of interfacial energy minimization. It seems clear, also, that the rate at which aqueous fluids (if not melts) are redistributed in nature can be quite rapid, since only minutes to hours are required to achieve consistent partitioning results in the laboratory at temperatures not greatly in excess of those expected in nature (although the rate of fluid re-distribution may depend on the solubilities of the minerals involved). This latter observation concerning the rate of fluid redistribution is consistent with the conclusions of Stevenson (1986), who argued that migration of aqueous fluids driven by gradients in surface tension might be extremely fast. The above conclusions may bear on a wide variety of processes, including melt localization and migration in the crust and upper mantle (at scales ranging from

millimeters to meters), aqueous fluid expulsion from (or retention in?) subducted slabs, and fluid redistribution and flow in metamorphic piles. The concept of metamorphic aquifers and aquitards (Ferry 1988) becomes entirely reasonable even in systems lacking fractures, simply because fluids could be effectively focused into rock units of particular composition and interfacial properties, imparting to those units unusually high permeabilities. Because fluid localization has been shown to occur at the scale of individual mineral grains (Fig. 15), it also seems plausible that development of large porphyroblasts (e.g., garnets?) in metamorphic rocks is aided by non-uniform fluid distribution: perhaps some crystals are simply better "nourished" than others through intimate contact with fluid.

Unfortunately, conclusions more specific than those described above would be premature at the present time because this study focused so heavily upon simple analog materials. The strong partitioning of aqueous fluid into clinopyroxenite

relative to quartzite is a sound geologic result. However, generalization to other systems—even ones consisting of quartz plus a different mafic mineral such as amphibole—is risky because the underlying cause of the fluid preference for pyroxene is uncertain (e.g., generally lower γ_{cf} for the pyroxenite, faceting of grains, or smaller mean grain size of clinopyroxene, etc?). The most serious limitation to generalization is the virtual lack of data on interfacial energies (γ_{gb} and γ_{cf}) for minerals: it is not even known, for example, whether clinopyroxenes and clinoamphiboles have similar values.

There are several potentially fruitful directions for future lithologic partitioning experiments on materials closely analogous to natural rocks. Perhaps foremost among these are samples incorporating aqueous fluid plus two or more minerals common in intermediate- to high-grade crustal metamorphic rocks (it would be ideal to experiment directly on realistic metamorphic assemblages, but in the writer view of the writer it will be difficult to achieve equilibrium microstructures at subsolidus temperatures—except possibly by resorting to extremely small grain sizes and using the TEM for image acquisition). Equally important with regard to aqueous fluid behavior are assemblages expected in and above the subducted slab [e.g., involving amphibole, clinopyroxene, and olivine (W.G. Minarik and J.M. Brenan, in preparation)]

More effort is also needed on partially molten systems. The one olivine/pyroxene/basalt experiment reported here indicates little or no melt partitioning effect in systems containing varying proportions of olivine and orthopyroxene. However, this one result cannot be considered definitive of partially molten upper mantle in general, if for no other reason than that the redistribution of melt will be more sluggish than that of aqueous fluid (Stevenson 1986), and a time series is needed. Lithologic distribution of melt during crustal fusion is still poorly understood as well, but given the measurable tendency to establish a minimum-energy melt fraction in migmatite analogs in the laboratory (Lupulescu and Watson 1999) there exists some hope of characterizing melt partitioning in similar systems.

Above all, data on grain-boundary and mineral/fluid interfacial energies are needed to advance the concepts put forth in this paper.

REFERENCES CITED

Ague, J.J. (1995) Deep crustal growth of quartz, kyanite and garnet into large-aperture, fluid-filled fractures, north-eastern Connecticut, USA. Journal of Metamorphic Geology, 13, 299–314.
Ayers, J.C., Brenan, J.M., Watson, E.B., Wark, D.A., and Minarik, W.G. (1992) A new capsule technique for hydrothermal experiments using the piston-cylinder apparatus. American Mineralogist, 77, 1080–1086.
Faul, U., Toomey, D.R., and Waff, H.S. (1994) Intergranular basaltic melt is distributed in thin, elongated inclusions. Geophysical Research Letters, 21, 29–32.
Ferry, J.M. (1988) Contrasting mechanisms of fluid flow through adjacent stratigraphic units during regional metamorphism, south-central Maine, USA. Contributions to Mineralogy and Petrology, 98, 1–12.
Holness, M.B. (1995) The effect of feldspar on quartz-H_2O-CO_2 dihedral angles at 4 kbar, with consequences for the behavior of aqueous fluids in migmatites. Contributions to Mineralogy and Petrology, 118, 356–364.
Holness, M.B. and Graham, C.M. (1991) Equilibrium dihedral angles in the system H_2O-CO_2-calcite, and implications for fluid flow during metamorphism. Contributions to Mineralogy and Petrology, 108, 368–383.
Jurewicz, S.R. and Watson, E.B. (1985) The distribution of partial melt in a granitic system: the application of liquid-phase sintering theory. Geochimica et Cosmochimica Acta, 49, 1109–1121.
Kelemen, P.B., Shimizu, N., and Salters, V.J.M. (1995) Extraction of mid-ocean-ridge basalt from the upwelling mantle by focused flow of melt in dunite channels. Nature, 375, 747–753.
Kingery, W.D., Bowen, H.K., and Uhlmann, D.R. (1976) Introduction to Ceramics (Second Edition). Wiley, New York.
Koga, K.T. (1993) Pore geometry in calcite-fluid system at high pressure-temperature conditions. EOS Transactions of the American Geophysical Union, 74, 325.
Laporte, D. and Watson, E.B. (1991) Direct observation of near-equilibrium pore geometry in synthetic crustal lithologies. Journal of Geology, 99, 873–878.
Lee, V.W., Mackwell, S.J., and Brantley, S.L. (1991) The effect of fluid chemistry on wetting textures in novaculite. Journal of Geophysical Research, 96, 10023–10037.
Lupulescu, A. and Watson, E.B. (1999) Melt segregation, part B. Minimum-energy melt fraction (MEMF)—implications for layered migmatite formation. Contributions to Mineralogy and Petrology, in press
McKenzie, D. (1987) The compaction of igneous and sedimentary rocks. Journal of the Geological Society of London, 144, 299–307.
Mibe, K., Fujii, T., and Yasuda, A. (1998) Connectivity of aqueous fluid in the Earth's upper mantle. Geophysical Research Letters, 25, 1233–1236.
Nakamura, M. and Watson, E.B. (1999) Fluid migration and texture development in a quartzite-water system. Transactions of the American Geophysical Union, 80, S319.
Park, H.H. and Yoon, D.N. (1985) Effect of dihedral angle on the morphology of grains in a matrix phase. Metallurgical Transactions A, 16A, 923–928.
Richter, F.M and McKenzie, D. (1984) Dynamical models for melt segregation from a deformable matrix. Journal of Geology, 92, 729–740.
Smith, C.S. (1964) Some elementary principles of polycrystalline microstructure. Metallurgical Reviews, 9, 1–48.
Stevenson, D.J. (1986) On the role of surface tension in the migration of melts and fluids. Geophysical Research Letters, 13, 1149–1152.
von Bargen, N. and Waff, H.S. (1986) Permeabilities, interfacial areas, and curvatures of partially molten systems: results of numerical models of equilibrium microstructures. Journal of Geophysical Research, 91, 9261–9276.
Waff, H.S. and Bulau, J.R. (1979) Equilibrium fluid distribution in an ultramafic partial melt under hydrostatic stress conditions. Journal of Geophysical Research, 84, 6109–6114.
Waff, H.S. and Faul, U. (1992) Effects of crystalline anisotropy on fluid distribution in ultramafic partial melts. Journal of Geophysical Research, 97, 9003–9014.
Wark, D.A. and Watson, E.B. (1998) Grain-scale permeabilities of texturally equilibrated, monomineralic rocks. Earth and Planetary Science Letters, 164, 591–605.
Watson, E.B. and Brenan, J.M. (1987) Fluids in the lithosphere. 1. Experimentally determined wetting characteristics of CO_2-H_2O fluids and their implications for fluid transport, host-rock physical properties, and fluid inclusion formation. Earth and Planetary Science Letters, 85, 497–515.
Watson, E.B. and Lupulescu, A. (1993) Aqueous fluid connectivity and chemical transport in clinopyroxene-rich rocks. Earth and Planetary Science Letters, 117, 279–294.
Watson, E.B. and Wark, D.A. (1997) Diffusion of dissolved SiO_2 in H_2O at 1GPa, with implications for mass transport in the crust and upper mantle. Contributions to Mineralogy and Petrology, 130, 66–80.